Migration and transformation of soil mercury in a karst region of southwest China: Implications for groundwater contamination

Jicheng Xia [a], Jianxu Wang [a], Leiming Zhang [b], Xun Wang [a], Wei Yuan [a], Tao Peng [a, d], Lirong Zheng [e], Weijun Tian [a, c], Xinbin Feng [a*]

[a] State Key Laboratory of Environmental Geochemistry, Institute of Geochemistry, Chinese Academy of Sciences, Guiyang 550081, China

[b] Air Quality Research Division, Science and Technology Branch, Environment and Climate Change Canada, Toronto, M3H5T4, Canada

[c] University of Chinese Academy of Sciences, Beijing, 100049, China

[d] Puding Karst Ecosystem Research Station, Chinese Academy of Sciences, Puding, 562100, China

[e] Beijing Synchrotron Radiation Facility, Institute of High Energy Physics, Chinese Academy of Sciences, Beijing 100049, China

* Corresponding author.

E-mail address: fengxinbin@vip.skleg.cn

Abstract

The slow pace of soil formation and thin soil thickness in karst regions limit the soil environmental capacity and are critical factors affecting the ecosystems' susceptibility in these regions. Guizhou Province is located in the heart of China's southwestern karst zone; its forest cover has doubled to over 60% of the whole area in the past two decades. Given the significant changes in land use in this province during the recent decades, the transport and transformation of soil Hg have likely changed, which may impact groundwater quality in karst environments. This study examines the vertical migration and transformation of soil mercury (Hg) in two karst catchments, Huilong and Chenqi with the former containing high Hg contents associated with mineralization and the latter representing regional background Hg. The results show that the soil Hg pool in the Huilong catchment was as high as 44.4±4.2 g m^{-2}, whereas in the Chenqi catchment was only 0.17±0.02 g m^{-2}. Compared with farmland soil, forest soil showed a significant loss of Hg. The results of L_3 X-ray absorption near edge

structure of Hg indicated that α-HgS, the primary mineral of Hg ore, gradually changed to other mineral types during soil formation. In Huilong catchment, the proportion of organic bound $Hg(SR)_2$ out of total Hg decreased from 44.0% to 20.3% when soil depth increased from 10 cm to 160 cm in farmland soil profile and from 39.3% to 34.5% in forest soil profile, while the proportion of ionic Hg increased with soil depth, from 4.2% to 10.7% in the farmland soil profile and from 6.7% to 11.6% in the forestland soil profile. Results from the triple-mixing isotope model show that soil Hg accounts for more than 80% Hg in groundwater in the two catchments. Our study indicates that the risk of soil Hg entering into groundwater in this karst area should not be ignored.

Keywords: Hg speciation, karst catchment, land use type, Hg stable isotopes, groundwater contamination

1. Introduction

Mercury is one of the most toxic heavy metal pollutants and can be transported globally by atmospheric processes (Driscoll et al. 2013). Karst ecosystems with high Hg background concentrations play a unique role in the global Hg biogeochemical cycle, especially for the fast flow into aquifers and associated risk of groundwater contamination (Xia et al. 2021a). The global Hg mineralization zone and karst concentration distribution area are highly overlapping in southwest China (see Figs. S1 & S2) (Gustin et al. 1999). China possesses the largest area of karst terrain in the world, and nearly half of the karst landforms in China are distributed in the southwestern part of the country (Huang et al. 2008)). The karst region of southwest China covers an area of 6.2×10^4 km^2 and is located on the global Hg mineralization belt, a region containing the majority of the Hg ore deposits in China. For example, Guizhou Province in this region, the most important Hg production base in China, possesses an estimated Hg reserve of 880,000 tons, accounting for about 78% of the national total (Qiu et al. 2009). The area is characterized by low temperature metallogenic ores associated with

numerous exposed low-temperature hydrothermal deposits. The mining and smelting of Hg and other mineral resources release large quantities of Hg to the surface environment.

Mercury contents in surface (0 - –25 cm) and deeper soils in the karst region of southwest China are 3–5 times higher than in the other regions of China, largely due to the region's high geochemical background Hg levels (Nie et al. 2019). The high background Hg contents associated with the region's contiguous karst landforms combined with extensive agricultural activities may negatively impact the region's function as an important ecological barrier that protects the middle and upper reaches of the Yangtze and Pearl Rivers. Specifically, excessive agricultural and mining activities may exacerbate the release of Hg into the atmosphere, water, and soil environments, and seriously affect the environmental quality and agricultural product safety of karst areas. In fact, human activities and other factors that enhanced soil erosion have resulted in an 84% increase in the loss of Hg from 1990 to 2010 in the karst areas of southwest China (Liu et al. 2019b). A better understanding of the biogeochemical cycling of Hg in the karst ecosystem is urgently needed in order to sustain future agricultural development while maintaining a health ecological environment.

Vegetation plays a key role in the biogeochemical cycling of Hg in terrestrial ecosystems. On the global scale, forest ecosystems are a net sink of atmospheric Hg, which absorb about 1,180 tons of Hg from the atmosphere annually (Wang et al. 2016). Agricultural cultivation strongly perturbs the biogeochemical cycling of Hg in terrestrial ecosystems. Guided by the government policy of building a green environment, the vegetation coverage in the karst areas has increased in recent years. For example, the forest coverage in Guizhou province has increased from 30% of the land area in 1998 to 60% in 2020. Such big land use change likely has impacts on Hg biogeochemical cycling in terrestrial ecosystems as well as to underground water quality.

The underground drainage network in the karst area is highly developed, while the thickness of the soil is relatively thin, limiting the region's capacity to resist environmental

damage (Xiao et al. 2021). Given the combined traits of an ecologically fragile karst ecosystem and high Hg background levels, the main factors controlling the migration of soil Hg and its transformation under different land use conditions in karst areas need to be better understood. These factors may play an important role in determining and preventing the risk of groundwater Hg pollution in karst areas (Bavec and Gosar 2016). This study intends to use chemical extraction and synchrotron radiation technology to assess the migration and transformation of soil Hg in karst catchments mediated by land use types, and to determine the main controlling factors for the transformation of soil Hg speciation under different types of conditions. Particularly, Hg stable isotope composition in precipitation, soils, runoff and associated environmental media were analyzed to understand the soil Hg fate in karst ecosystem. Mercury in soil profiles under different geological background conditions and land use types was analyzed in detail in terms of Hg distribution, speciation and stable isotope compositions to better understand the vertical migration and transformation of soil Hg and its potential impacts to groundwater in karst areas. Knowledge gained in this study is useful for developing future land use management and Hg emission control policies in order to sustain future agricultural development while maintaining a healthy ecological environment.

2. Materials and Methods

2.1 Sites descriptions

The two karst catchments in southwestern China, Huilong and Chenqi, were selected in a previous study to assess the source and sink of Hg using a mass balancing approach (Xia et al. 2021a). The same two catchments were also selected in the present study to investigate the migration and transformation of soil Hg under different land use. Briefly, the Huilong catchment is located in the southwestern part of Guizhou Province, whereas the Chenqi catchment is located in the central part of the province (Fig. S3), and they are underlain by detrital sandstone and limestone, respectively (Sun et al. 2012; Zhao et al. 2010). Mercury mining occurred in the Huilong catchment continued for about 350 years and ceased in the

1950s, but there are no known Hg deposits in Chenqi (Wang et al. 2005). These two catchments are representative of the region, with the former having higher and the latter having lower Hg (or background) levels. More information about these two catchments can be found in Xia et al. (2021a).

2.2 Sampling and measurement

The locations for soil profile sampling were selected based on the distributions of forests- and farmlands within the catchment. Two locations were selected within each catchment, one for forest soil and another for agricultural soil. Soil and bedrock sampling were performed with a circular knife/geological hammer from top to bottom to avoid contamination. The soil and bedrock samples were put into sample bags, numbered, and shipped to the laboratory for drying at 40℃. The samples were weighed and recorded, and the visible plants, stones and other sundries were removed from the samples. After grinding, the soil and bedrock samples were screened through a 200-mesh sieve. The materials were then separated and recorded for further chemical analysis. An Hg analyzer DMA80 (Milestone Ltd. Italy) was used to determine the total Hg content in the collected soil and bedrock samples. The method's detection limit is 0.01 ng g^{-1}. The average relative standard deviation for the duplicate analyses of Hg was 4.7%. Matrix spiked recoveries ranged from 92% to 105% (mean=97%, n=6). The equipment blank for Hg in liquid samples was 0.05 ± 0.01 ng L^{-1} (n=6). The soil reference material GBW07405 was used for soil analytical quality control. The measured average Hg content of the reference materials was 0.27 ± 0.09 mg kg^{-1} (n=6), which was comparable to the certified value of 0.29 ± 0.04 mg kg^{-1}. The relative percentage differences between the sample replicates were <7%.

The sampling and measurement for associated samples, such as throughfall, rainfall, surface runoff and groundwater were described in detailed addressed in Xia et al. (2021a). Briefly, samples of bedrock, soils, water and chlorinated activated carbon pre-enriched samples for isotopic analysis were pre-concentrated in a dual temperature-controlled tubular

muffle furnace, and the Hg released by thermal decomposition was treated with 5 ml of 40% aqua regia (v:v, HNO_3:HCl) absorption liquid capture (Li et al. 2019). The Hg concentrations of the absorbing liquid was determined according to the method of USEAP 1631 with a Hg analyzer Tekran 2500 (Tekran Ltd, CA), and the detection limit of this method was 0.2 ng L^{-1}. The method recoveries of pretreatment were tested by using standard reference materials BCR-482 (480±20 μg kg^{-1}) and GSS-4 (590±50 μg kg^{-1}), which were 92.1±3.5% (n=6) and 94.5±4.7% (n=6), respectively.

2.3 Determination of chemically extracted soil Hg

Mercury in some soil samples was extracted according to the BCR continuous extraction method proposed by the European Agency for Material Standards. Mercury speciation was assessed, in part, using a chemical sequential extraction method (Quintanilla-Villanueva et al. 2020). Detailed steps see supplementary information text.

2.4 X-ray absorption near-edge structure spectrum of Hg L_3

About 0.1 g of the sieved soil or bedrock sample was placed into a special tablet press (FW-4, Tianguang Instruments, China) to create a sample pellet, Φ=1 cm. The reference compounds selected in this study were based on the existing literature pertaining to soil and Hg components (Yin et al. 2016) and included cinnabar (α-HgS), metacinnabar (β-HgS), synthetic organic bound Hg ($Hg(SR)_2$), nano β-HgS, and ionic Hg ($HgCl_2$). The method used to determine the synthetic organic bound Hg ($Hg(SR)_2$) and nano-β-HgS is detailed in Liu et al. (2019a). The experiment was conducted at the 1W1B line station of the Beijing Synchrotron Radiation Facility (BSRF). The basic experimental parameters were set at 2.5 GeV of electron energy, 250 mA of electron current, and an energy resolution (ΔE/E) of 1-3×10^{-4}. For Hg L_3-edge XANES spectroscopy analyses, an energy range of 12.18-12.58 KeV was used to acquire the spectra. Data for Hg reference compounds were collected in transmission mode (Hg content>5%), and for sample pellets in fluorescence mode using a 19-element high-purity Ge solid-state detector under ambient conditions (soil matrix; 15 mg kg^{-}

[1]<Hg content<0.1%). Data normalization (background correction), and linear combination fitting (LCF) were performed with the IFEFFIT software package (Ravel and Newville 2005). The Hg L_3-edge XANES spectra of the standards and samples were plotted with the energy ranged between 12.20 and 12.58 KeV, as described in Wang et al. (2020).

2.5 Determination of Hg stable isotope compositions

Before determination of Hg stable isotope compositions, the Hg solution was diluted to 1 ng mL^{-1}. The preconcentration recoveries of BCR-482 (480±20 μg kg^{-1}, moss reference standard) and samples were all in the range of 95%-103%. The Hg isotopic composition was determined by a Nu II multi-receiver plasma mass spectrometer (Nu Instruments, UK) with a gas-liquid separation system HGX-200 (Teledyne CETAC Technologies, USA) and a desolvation nebulizer (CETAC Ardius) (Yin. et al. 2010). Gaseous elemental Hg was generated online from Hg standard sample or test sample by using $SnCl_2$ (3%) as the reducing agent of Hg. Instrument mass bias correction was performed using internal standards (NIST 997) and external standards (NIST 3133).

Mercury isotope mass-dependent fractionation (MDF) is expressed as δ(‰) and is calculated as follows:

$$\delta^{202}Hg(‰) = 1000 \times [(^{202}Hg/^{198}Hg_{sample})/(^{202}Hg/^{198}Hg_{NISTSRM3133}) - 1] \quad (1)$$

The mass-independent fractionation (MIF) of Hg isotopes is represented by Δ(‰), and is calculated as follows:

$$\Delta^{199}Hg\ (‰) \approx \delta^{199}Hg - 0.2520 \times \delta^{202}Hg \quad (2)$$

$$\Delta^{200}Hg\ (‰) \approx \delta^{200}Hg - 0.5024 \times \delta^{202}Hg \quad (3)$$

$$\Delta^{201}Hg\ (‰) \approx \delta^{201}Hg - 0.7520 \times \delta^{202}Hg \quad (4)$$

$$\Delta^{204}Hg\ (‰) \approx \delta^{204}Hg - 1.4930 \times \delta^{204}Hg \quad (5)$$

One UM-Almadén solution was inserted as an internal standard for every 10 samples. In order to evaluate whether the pretreatment process such as pyrolysis-pre-enrichment will lead to obvious isotopic bias, the reference standard materials BCR-482 and GSS-4 were

183 determined several times during the sampling period. Results of UM-Almaden (δ^{202}Hg = –
184 0.53 ± 0.08‰, Δ^{199}Hg = –0.01 ± 0.05‰, Δ^{201}Hg = –0.02 ± 0.07‰, 2 SD, n = 8) and BCR-482
185 (δ^{202}Hg = –1.55 ± 0.09‰, Δ^{199}Hg = –0.58 ± 0.06‰, Δ^{200}Hg = –0.01 ± 0.03‰, Δ^{201}Hg = –0.59
186 ± 0.08‰, 2 SD, n = 3) are consistent with previously reported values, indicating that both the
187 instrument precision and the sample pretreatment method were reliable (Blum and Bergquist
188 2007).

189 No significant odd or even MIF occurred during dissolution, but MDF was present (Drott
190 et al. 2013; Wiederhold et al. 2015). Therefore, for the hydrological process that only includes
191 leaching, dissolution and scrubbing, Δ^{199}Hg and Δ^{200}Hg can be used to calculate the
192 endmember ratio. With two degrees of freedom, the contribution ratio of the three
193 endmembers can be calculated at the same time. A triple-mixing isotope model was thus used
194 to quantify the contribution of potential groundwater Hg inputs (e.g., rainfall Hg, throughfall
195 Hg, and soil Hg). Monte Carlo simulation was applied to generate one million groups of
196 Δ^{199}Hg and Δ^{200}Hg, which randomly ranging from Mean –SD to Mean +SD (Wang et al.
197 2019). The fraction ratio is estimated as the average of these solutions, which is in the range
198 of 0–1, based on one million times of solutions of Eqs. (6-8).

199 $$f_1\times\Delta^{199}Hg_1+f_2\times\Delta^{199}Hg_2+f_3\times\Delta^{199}Hg_3=\Delta^{199}Hg_{groundwater} \quad (6)$$

200 $$f_1\times\Delta^{200}Hg_1+ f_2\times\Delta^{200}Hg_2+f_3\times\Delta^{200}Hg_3=\Delta^{200}Hg_{groundwater} \quad (7)$$

201 $$f_1+f_2+f_3=1 \quad (8)$$

202 *2.6 Soil organic matter, pH, zirconium and migration coefficient*

203 To determine the organic matter content of the soil samples, standard solutions of
204 potassium dichromate (1.0 mol L^{-1}) and ferrous sulfate (0.2 mol L^{-1}) were prepared,
205 following the method described (Li et al. 2021) . The percent of soil organic matter was then
206 calculated as:

207 $$SOM\ (g\ kg^{-1}) = (V_0\text{-}V) \times C_{FeSO4}\times 0.003\times 1.724\times F\times 1000/W \quad (9)$$

where V_0 is the volume of $FeSO_4$ solution (mL) consumed in the blank test; V is the volume of $FeSO_4$ solution (mL) consumed during sample analysis; C_{FeSO4} is the molar concentration of the standard solution; 0.003 is the molar mass of 1/4 carbon atom (g mol^{-1}); 1.724 is a factor needed to convert organic carbon into organic matter (calculated according to the average carbon content of soil organic matter, 58%); W is the weight of dried soil sample (g); and F is the oxidation correction coefficient, which is determined according to the soil organic matter content. When F is ≤ 1% before correction, it is given a value of 1.25; otherwise, it is 1.16.

Ultra-pure water was used as the extraction solution (Xie et al. 2017), and the ratio of extraction solution to soil was 2.5:1. 10.0 g of processed soil sample (weighed with an accuracy of 0.1 g) was put into a 50 mL plastic centrifuge tube, and 25 mL of ultra-pure water was added. The tube was then oscillated on an oscillator for 10 min and allowed to stand for 30 min. A corrected glass pH meter electrode was then placed into the tube, and the pH of the solution was recorded.

Soil and bedrock zirconium contents were analysed using inductively coupled plasma mass spectrometry, as detailed in Xia et al. (2021b).

The migration coefficient (*MC*) can be used to describe the migration and enrichment characteristics of Hg in the soil profile relative to the bedrock (Nesbitt 1979; Sun et al. 2019), and was calculated as:

$$MC = \frac{C_{S-Hg}}{C_{S-Zr}} \times \frac{C_{R-Zr}}{C_{R-Hg}} - 1 \quad (11)$$

where $C_{S\text{-}Hg}$ and $C_{S\text{-}Zr}$ are the Hg and zirconium content in the soil and $C_{R\text{-}Hg}$, and $C_{R\text{-}Zr}$ are those in the bedrock, respectively. Zirconium was chosen as a reference element because of zircon's excellent stability to weathering results from its exceptionally low solubility in aqueous solutions (Santos et al. 2019). A *MC*>0 indicates that the sampling point is enriched

232 in Hg during the soil-forming process while a $MC<0$ indicates the Hg in the sampling point is
233 depleted.

234 **3. Results and Discussion**

235 *3.1 Distribution of Hg in soil profiles*

236 The soil Hg contents in the farmland and forested sections of the Huilong catchment were
237 97.9±51.3 mg kg^{-1} and 20.0±4.9 mg kg^{-1}, respectively, and those in the Chenqi catchment
238 were 0.16±0.05 mg kg^{-1} and 0.21±0.19 mg kg^{-1}, respectively. Soil Hg content in the farmland
239 section of the Huilong catchment slightly decreased with soil depth beneath the H-A-O (Fig.
240 1a). The soil closer to the surface is affected more by agricultural practices (such as
241 fertilization) as well as atmospheric deposition of Hg (Ma et al. 2022). Soil Hg content
242 gradually increased from the bottom of the H-A-O to the H-A-B, likely due to the downward
243 leaching and migration of Hg from the upper soil layer. Soil Hg content increased
244 significantly with soil depth in the H-A-C, presumably because of its proximity to the parent
245 material that possessed relatively high Hg concentrations. Soil Hg content in the forestland
246 section of the Huilong catchment decreased with soil depth from the H-F-O to H-F-A (Fig.
247 1b). Mercury leaching was likely related to the layers with low soil pH (between 4 and 5). At
248 greater soil depths, Hg began to accumulate and soil Hg content increased.

249 Soil Hg content in the farmland section of the Chenqi catchment was relatively high in the
250 C-A-O (Fig. 1c), possibly because of Hg input from agricultural ploughing and atmospheric
251 Hg deposition. From the lower part of the C-A-O to the C-A-A, a portion of easily dissolved
252 Hg migrated downward through soil seepage, and was subsequently fixed in the C-A-B. Soil
253 Hg content changed little with soil depth in the bottom soil, which may be related to the low
254 geological background Hg in this area of the Chenqi catchment and absence of exogenous Hg
255 input or human activities. Soil Hg content in the forestland section of the Chenqi catchment
256 exhibited high concentrations in the C-F-O (Fig. 1d), which was mainly due to litterfall Hg
257 input. Soil Hg content decreased with soil depth in the C-F-A due to Hg leaching. Soil Hg

content increased with soil depth in the C-F-B due to the migration of Hg from the upper soil layer.

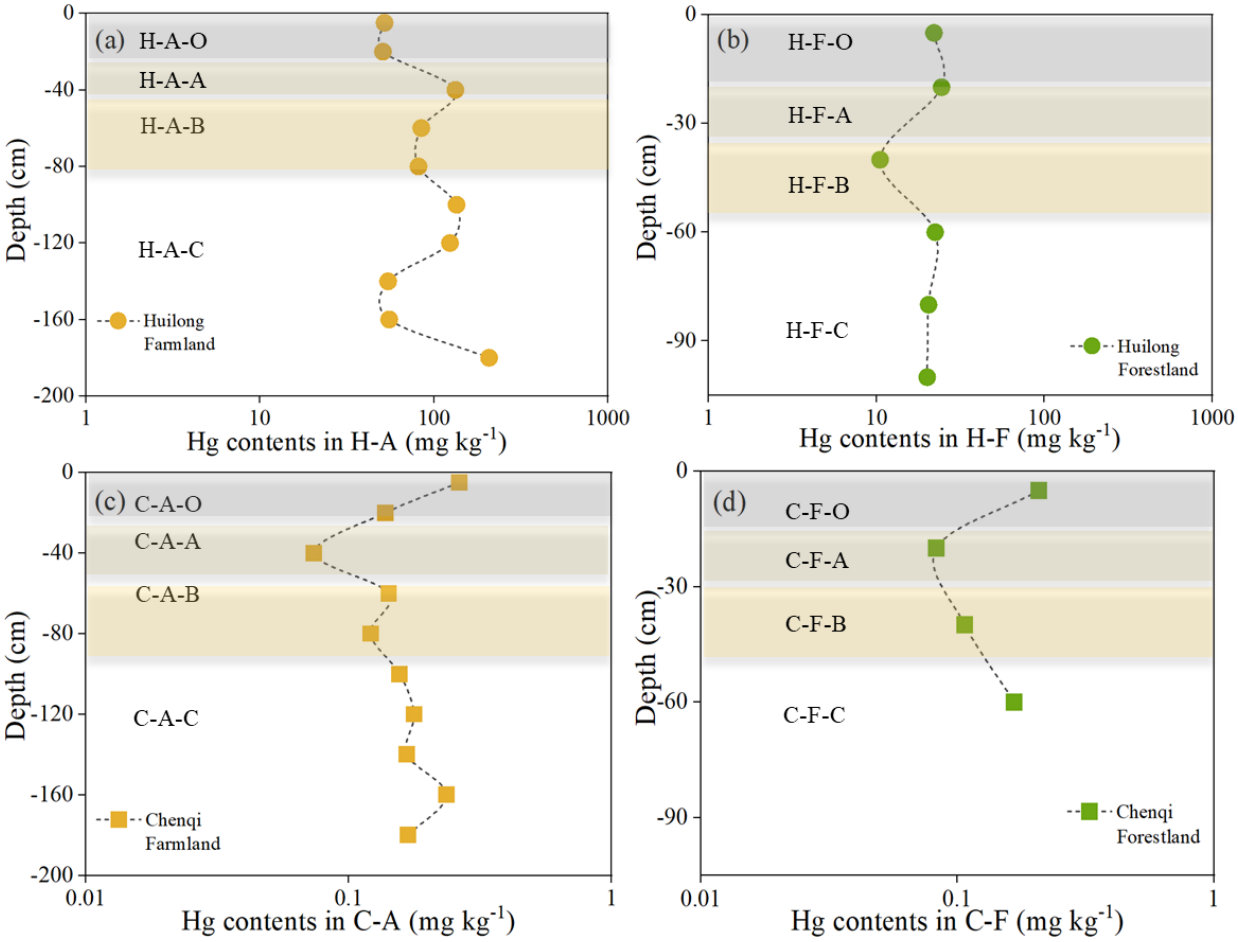

Fig. 1 Distribution of soil Hg content in the farmland (a) and forestland (b) sections of the Huilong catchment and in the farmland (c) and forestland (d) sections of the Chenqi catchment. H-A-O, H-A-A, H-A-B and H-A-C (C-A-O, C-A-A, C-A-B and C-A-C) represent the plough layer, leaching layer, deposition layer and parent layer of farmland soil profile in the Huilong (Chenqi) catchment, respectively; H-F-O, H-F-A, H-F-B and H-F-C (C-F-O, C-F-A, C-F-B and C-F-C) represent the organic matter layer, leaching layer, deposition layer and parent layer of forestland soil profile in the Huilong (Chenqi) catchment, respectively.

3.2 Mercury migration and accumulation in the karst soil profiles

In this study, the migration and accumulation of Hg in the farmland and forestland soil profiles of the Huilong and Chenqi catchments were characterized using a migration

coefficient (*MC*) (Fig. 2a). The farmland soil profile within the Huilong catchment possessed two distinct ranges of *MC* values: *MC* >0 and *MC* <0. *MC* is in the range of -0.9 – 0.0 at soil depths of 0–80 cm and 130–180 cm, indicating that soil Hg at these depths is relatively depleted. This suggests that the shallow and deep seepage of water through the soil has leached the soil Hg within these two soil layers (Abu-Dieyeh et al. 2019). In addition, Hg may have been lost from the soil surface by interfacial Hg exchange with the atmosphere. Since the background soil Hg concentrations are as high as several hundreds of mg kg^{-1} in this area, the magnitude of the interfacial Hg exchange between soil and atmosphere interface is likely large and result in Hg loss from soil (Qiu et al. 2006). *MC* is in the range of 0.0 – 0.9 at soil depths of 80 –130 cm, indicating that soil Hg at these depths is relatively enriched. Mercury enrichment may be due to the downward transport of Hg from the upper layer and its subsequent redeposition.

For the forest soil profile of the Huilong catchment, soil Hg was relatively depleted in general with *MC* being in the range of -0.75 – 0.0 (Fig. 2b). In the organic layer (0 – 20 cm soil depth), the degree of Hg loss was limited (*MC*: -0.54 – -0.45), likely due to the release of Hg from leaf litterfall degradation that supplements the soil Hg. The degree of Hg loss is relatively large between 40–60 cm depth (*MC*: -0.75 – -0.71) due to strong leaching and no effective supplementation of Hg. The depletion of Hg decreases at depths closer to the bedrock, likley due to higher Hg concentrations derived from the bedrock and retained in the regolith and semi-regolith near the bedrock.

In the farmland soil profile of the Chenqi catchment, soil Hg was enriched at all depth, with *MC* being in the range of 0 – 1.64 (Fig. 2c). The farmland is located in lower topographic areas of the catchment, and therefore continuously receives and accumulats Hg from eroded soil transported by surface runoff from areas of higher terrain and steeper slopes. The enrichment of Hg in the topsoil may also be related to atmospheric deposition and/or agricultural inputs. In the accumulation layer of the soil profile between 30–60 cm in depth,

MC increased significantly, reaching values as high as 1.6. The very high *MC* values at these depths indicate highly enriched Hg, presumably due to leaching from overlying soil (Teršič et al. 2014).

Soil Hg in the forest soil profile of the Chenqi catchment was relatively depleted in general (Fig. 2d), with *MC* being in the range of −0.7 – 0.0. In the organic layer (0 and 20 cm depth), the degree of Hg loss was relatively weak, possibly because of supplemental Hg released from leaf litterfall degradation (Silva-Filho et al. 2006). Soils between 20–40 cm depth exhibited a large degree of Hg loss (Fig. 2d), suggesting strong leaching while with limited Hg supplementation. The depletion of Hg decreases at depths closer to the bedrock, which may be because the soil at the bottom of the profile was not fully developed, limiting Hg migration at this depth.

In general, farmland soils in catchment depressions were close to 2 meters in thickness. Mercury in the deep soils shows varying degrees of depletion or enrichment depending on the superposition of factors such as the contributions of Hg from bedrock weathering, soil seepage and leaching, among others. Considering that lower pH should enhance Hg leaching (Soleh Setiyawan et al. 2020), soil pH might have also played an important role in shaping the soil Hg profile, knowing that soil pH of Huilong catchment is between 4.24 and 6.98 and that of Chenqi catchment is between 6.93 and 7.61 (Table S2). The thickness of the forest soil layer on the hillside is less than 1 meter. The thin soil layer could be caused by prominent soil erosion and large hill slopes in the karst area, both factors were conducive to Hg leaching through surface runoff and internal soil seepage. The reduced Hg loss in the organic soil layer should be related to the replenishment of soil Hg from litterfall input (Xia et al. 2021a).

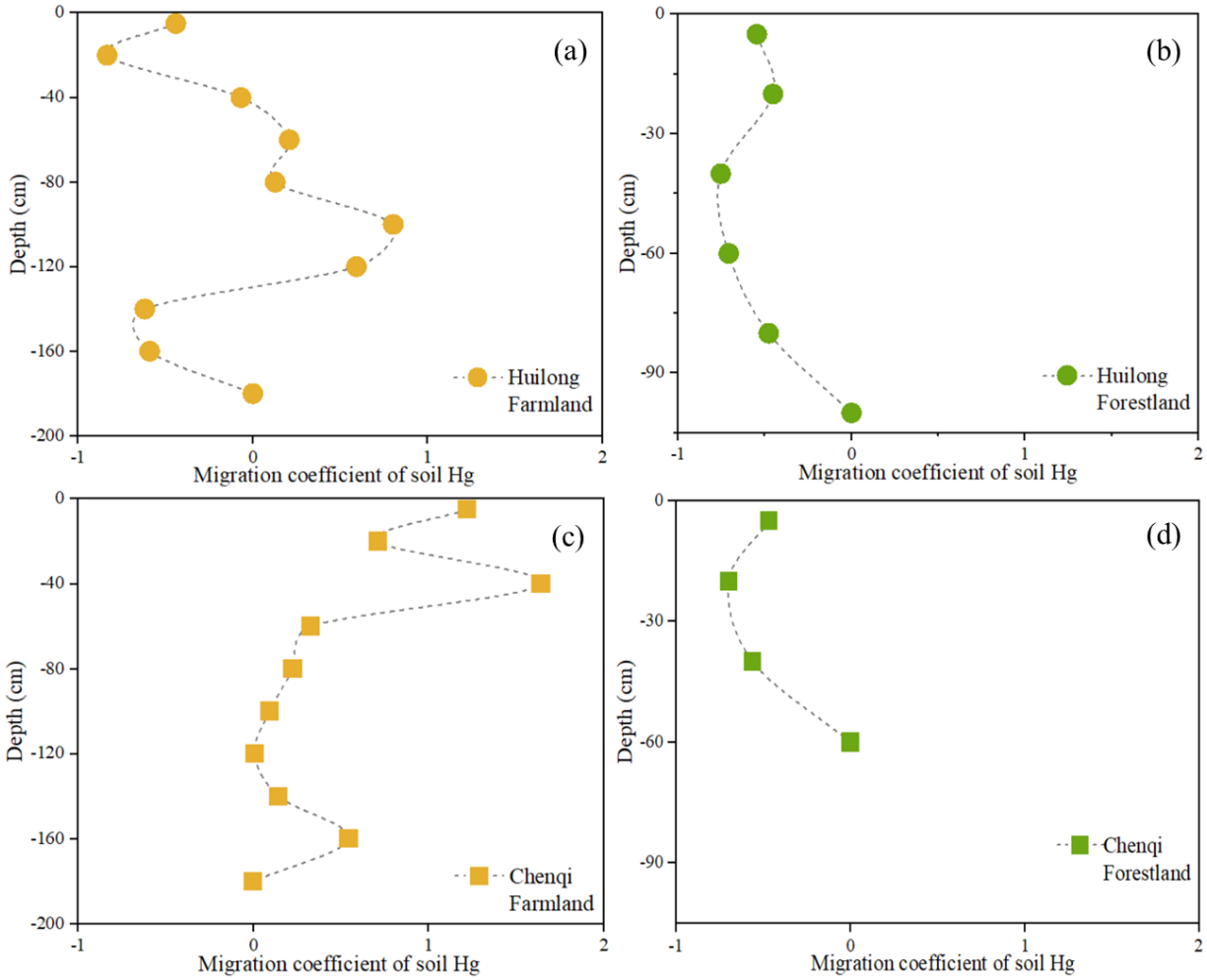

Fig. 2 Migration coefficient (*MC*) of soil Hg in Huilong and Chenqi catchments.

3.3 Chemically extracted Hg

Based on chemical sequential extraction data (Fig. 3), the proportions of Hg associated with the weak acid extraction phase were less than 0.7% and 1% of the total Hg in Huilong and Chenqi catchment, respectively, those of reducible Hg were less than 3% in both catchments, those of oxidizable Hg were 36.5%–76.1% and 25.5%–77.1%, respectively, and those of residual Hg were 23.5%–59.9% and 20.4%–70.7%, respectively.

In the farmland soil profile of the Huilong catchment, the weak acid extracted Hg (F1), reducible Hg (F2), and residual Hg (F4) increased, while the proportion of oxidizable Hg (F3) decreased from the H-A-O to the H-A-A, and to the H-A-B. In the forestland soil profile of the same catchment, F2 and F4 increased, while F3 decreased from the H-F-O to the H-F-A.

SOM decreased from 59.5 g kg^{-1} in the H-A-O to 29.3 g kg^{-1} in the H-A-A, and to 14.6 g kg^{-1} in the H-A-B (Fig. 3a).

In the Chenqi farmland soil profile (Fig. 3b), the proportions of weak acid extracted Hg (F1), reducible Hg (F2), and residual Hg (F4) increased with depth from the C-A-O to the C-A-B, whereas the proportion of oxidizable Hg (F3) declined. In the forestland soil profile, F2 and F4 increased from C-F-O to C-F-A, but F3 declined with depth. SOM has been shown to significantly affect the species of soil Hg (Gruba et al. 2019).

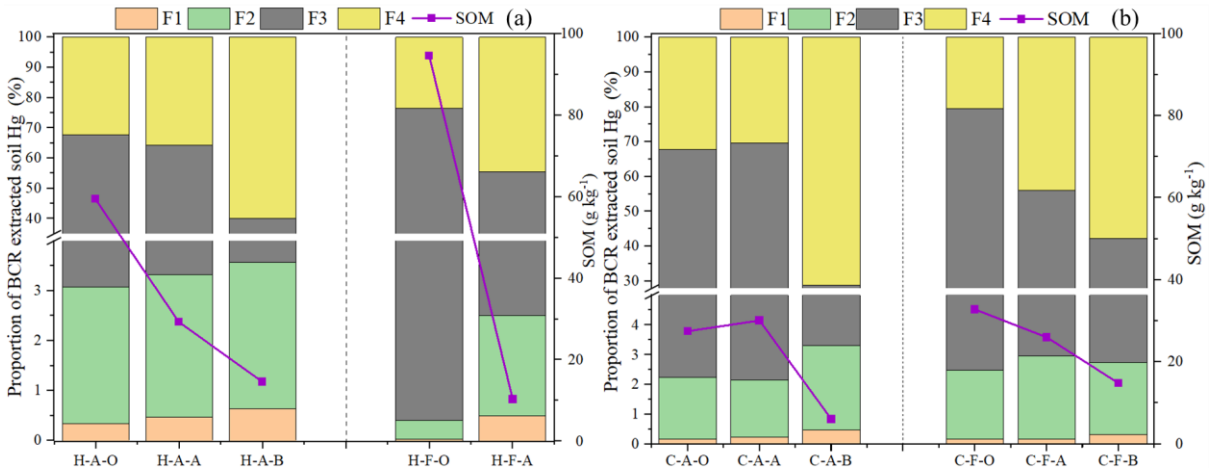

Fig. 3 Distribution of extracted soil Hg and SOM in the farmland and forestland soil profiles of the two catchments. H-A-O, H-A-A and H-A-B (C-A-O, C-A-A and C-A-B) represent the plough layer, leaching layer and deposition layer of farmland soil profile in the Huilong (Chenqi) catchment, respectively; H-F-O and H-F-A (C-F-O and C-F-A) represent the organic matter layer and leaching layer of forestland soil profile in the Huilong (Chenqi) catchment, respectively. C-F-B represents the deposition layer of the forest soil profile in the Chenqi catchment.

3.4 Mercury speciation in the soil profiles determined by XANES

Data obtained from the synchrotron radiation near-side absorption spectrum for the farmland soil profile in the Huilong catchment (Fig. 4) showed that organically bound Hg decreased from the surface H-A-O to the H-A-A, and to the H-A-B. The proportion of $Hg(SR)_2$ in these three layers was 44.0%, 23.2% and 20.3%, respectively, similar to those of organically bound Hg extracted by the BCR. The high proportion of organically bound Hg in

354 the cultivated layer of the soil may be related to long-term agricultural farming activities,
355 including the addition of straw and fertilization to the farm field. The application of livestock
356 manure may be particularly important. In the Huilong catchment, the annual average yields of
357 corn stalks and barley stalks were as high as 20250 and 6750 kg ha^{-1} yr^{-1}, while their Hg
358 contents were 0.32±0.05 mg kg^{-1} and 0.15±0.03 mg kg^{-1}, respectively (Xia et al. 2021a). A
359 portion of the harvested straw is naturally degraded and incorporated into the soil as it is
360 returned to the fields. The remaining portion of straw is usually recycled by farmers to feed
361 livestock, and the resulting farmyard manure is applied to the farmland. Thus, while the soil
362 fertility of the cultivated layer is improved, the content of organically bound Hg in the soil is
363 always maintained at a high level. $Hg(SR)_2$ is potentially bioavailable, especially when the
364 soil is acidic. Soil Hg in the form of $Hg(SR)_2$ could increase Hg contents in crop products,
365 and subsequently increase the risk of Hg exposure by local residents consuming products.
366 Meanwhile, $Hg(SR)_2$ in soil could also increase the possibility of Hg conversion to ionic Hg,
367 which will increase the potential downward migration of Hg from the upper soil layers by
368 leaching.

369 The proportion of ionic Hg increased gradually with soil depth from 4.2% to 6.9%, and
370 then to 10.7% (Fig. 4), similar to the change in the proportion of weak acid extracted Hg and
371 reducible Hg as determined by BCR, and this may be related to soil pH and SOM. The acidic
372 nature of the soil at Huilong likely allows for significant leaching, resulting in continuous
373 accumulation and increasing proportions of ionic Hg from the top to bottom of the soil
374 profile. This trend is consistent with observed downward increase in organic matter content
375 (Fig. 4). The ionic Hg that can be combined and fixed by the organic matter decreases,
376 suggesting that with continued leaching of ionic Hg the sorption capacity of the organic
377 matter becomes saturated, allowing Hg to be transported to greater depths (McLagan et al.
378 2022). A considerable amount (ranging from a few percent to a dozen percent) of ionic Hg
379 has been observed in the soils of several world-famous Hg mining districts (such as Almadén,

Asturias (Spain), Idria (Slovenia) and Wanshan (China)) (Esbri et al. 2010; Yin et al. 2016). Soils characterized by high Hg background content and intensive soil leaching of ionic Hg increases the risk of the downward migration of soil Hg to groundwater.

The proportion of α-HgS increases toward the deep soil from 8.5% to 9.3%, and to 21.0%. α-HgS was the main component of natural Hg ore. The content of this form of Hg tends to decrease with soil formation. It may be transformed to other forms of Hg by biologically-mediated weathering (Gómez-Armesto et al. 2020). The closer the soil is to the surface, the stronger the weathering is and the more primary minerals are degraded, thereby reducing the portion of soil Hg as α-HgS (Bourdineaud et al. 2020).

The proportions of β-HgS in the H-A-O and H-A-A were 13.6% and 9.3%, respectively, whereas those of nano β-HgS were 26.8% and 50.0%, respectively. A possible factor producing the opposite trends between β-HgS and nano β-HgS is the transformation of nano β-HgS, which is an amorphous Hg sulfide. Soil weathering, especially in the cultivated layer that is strongly disturbed by farming, may promote the transformation of Nano β-HgS into more stable β-HgS.

In the forestland of the Huilong catchment, the proportion of organically bound Hg ($Hg(SR)_2$) declined slightly from 39.3% in the H-F-O to 34.5% in the H-F-A. This observed downward trend may be due to the accumulation of Hg in the surficial soil organic layer of the forestland from degradation of litterfall where the soil organic matter is constantly being renewed. The Hg flux from litterfall input in the Huilong catchment was estimated to be 129±85.3 μg m^{-2} yr^{-1} (Xia et al. 2021a). Most of the Hg derived from the degradation of litterfall will be incorporated into the soil, allowing organically bound Hg in the surface soil to be maintained at a relatively high level. The proportion of ionic Hg increased significantly, from 6.7% in the H-F-O to 11.6% in the H-F-A. The observed trend may be controlled by soil pH and SOM as described for the farmland soil. It may also be related to the greater moisture content of the forestland soils, which have a natural advantage in water retention in

comparison to adjacent non-forestlands (Monteiro Venturini et al. 2022). The tall forest canopy reduces solar radiation reaching to the surface, thereby reduces temperature and evaporation rate of soil water, which leads to higher soil moisture content that is conducive to leaching. In contrast to the farmland soil profile, the proportion of α-HgS in the forestland profile initially decreases by a large amount and then increases at greater depths (Fig. 4). The sharp decrease may be due to the lack of a plough layer in the surface soil that has been disturbed by anthropogenic activities over the years. In addition, the top layer of the forest was characterized by litterfall, and there was more bedrock in the bottom layer. α-HgS in the A-horizon is affected by its higher water content and by its well-developed plant root system that strengthens the effects of soil weathering and leaching. Thus, the primary minerals in this layer were α-HgS, which will be transformed into other forms of secondary minerals under strong weathering and leaching conditions. The limited weathering within the H-F-C results in a large proportion of the primary mineral α-HgS, which accounts for 85.4% of the total, leaving the remaining 16.9% as β-HgS.

In general, SOM was closely related to the oxidizable Hg. In the process of soil formation, the main primary mineral α-HgS of the Hg ore gradually changed to other mineral types. As the soil depth increases, the proportion of $Hg(SR)_2$ decreases, while the ionic Hg tends to increase. It was worth to note that the increasing tendency of ionic Hg with increasing soil depth implies that the risk of soil Hg entering groundwater was high in the karst areas with high Hg background. Therefore, both soil Hg profile and possible migration of Hg to groundwater need to be closely monitored in order to develop effective control measures to prevent soil Hg pollution to groundwater.

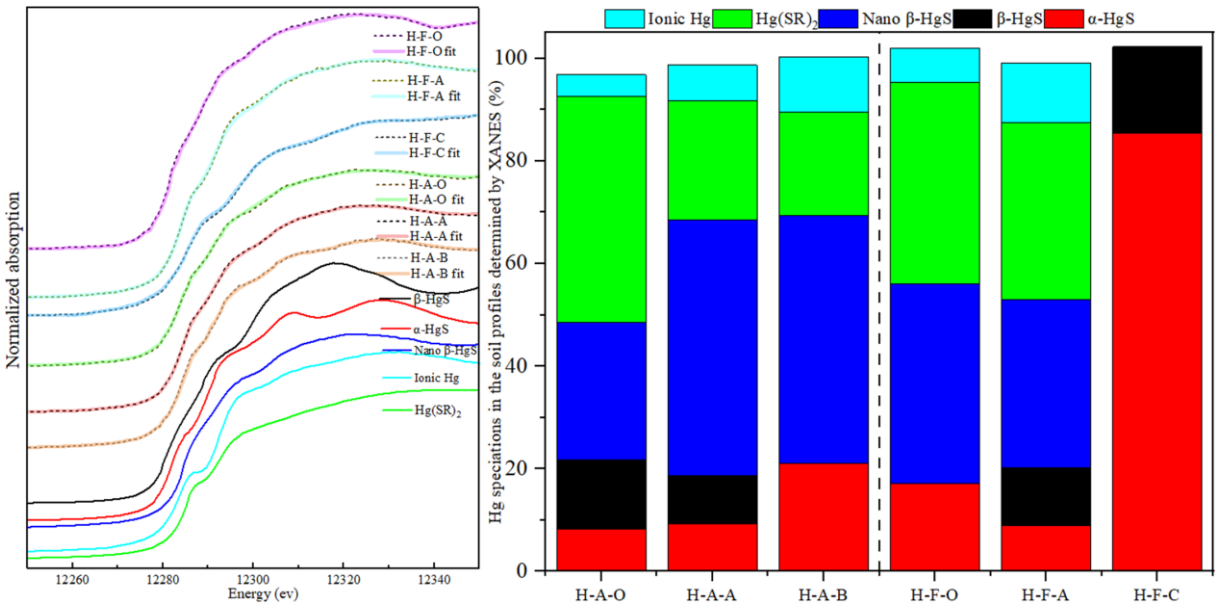

Fig. 4 XANES analysis of soil Hg in farmland and forestland profiles in the Huilong catchment. H-A-O, H-A-A, and H-A-B represent the plough layer, leaching layer, and deposition layer of farmland soil profile in the Huilong catchment, respectively; H-F-O, H-F-A, and H-F-C represent the organic matter layer, leaching layer, and parent layer of forestland soil profile in the Huilong catchment, respectively.

3.5 Mercury isotopic signatures in karst hydrological processes

The Hg isotopic signatures of rainfall in Huilong were δ^{202}Hg=-1.00±0.61‰, Δ^{199}Hg=0.48±0.19‰ and Δ^{200}Hg=0.13±0.05‰ (n=8), and those of throughfall were δ^{202}Hg=-1.77±0.47‰, Δ^{199}Hg=-0.06±0.11‰, and Δ^{200}Hg=0.02±0.03‰ (n=8) (Fig. 5a). The Hg isotopic signatures of rainfall in Chenqi were δ^{202}Hg=-0.42±0.14‰, Δ^{199}Hg=0.29±0.17‰ and Δ^{200}Hg=0.12±0.03‰ (n=5), and those of throughfall were δ^{202}Hg=-1.44±0.60‰, Δ^{199}Hg=-0.07±0.16‰ and Δ^{200}Hg=0.07±0.04‰ (n=11) (Fig. 5b). Note that the Hg isotopic signatures of natural precipitation in the global background area were δ^{202}Hg=-0.57±0.48‰, Δ^{199}Hg=0.44±0.23‰ and Δ^{200}Hg=0.25±0.19‰ (Chen et al. 2012; Demers et al. 2013). The MDF of Hg isotopes in the Chenqi catchment is slightly negative, and the MIF of Hg isotope was also significantly negative by about 0.2‰, which was likely due to the significantly higher Hg concentration in the precipitation in Chenqi (7.9–26.0 ng L^{-1}) compared to those of the forest precipitation in the global background area (5.9–19.0 ng L^{-1}) (Fu. et al. 2010; Xia et

al. 2021a). The Hg isotopic signatures observed in Chenqi reflect the influence of anthropogenic Hg sources that have negative δ^{202}Hg, and close to 0 Δ^{199}Hg and Δ^{200}Hg (Blum et al. 2014). Besides, a portion of the Hg isotopic signatures of the throughfall was inherited from those of the vegetation canopy due to the washout of particulate Hg adsorbed on the surface of leaves and trunks by throughfall. The Hg isotopic signatures of the vegetation canopy were characterized with negative δ^{202}Hg, Δ^{199}Hg and close to 0 Δ^{200}Hg (Demers et al. 2013). In conclusion, the Hg isotopic signatures of the forest soil do not have positive Δ^{200}Hg, and the Δ^{199}Hg signal was further diluted. Such a finding was of great significance for tracing the Hg cycle in the hydrological process of the karst area.

The Hg isotopic signatures of bulk soil were δ^{202}Hg=-0.29±0.24‰, Δ^{199}Hg=0.01±0.06‰ and Δ^{200}Hg=0.02±0.03‰ (n=11) in Huilong catchment (Fig. 5a), and were δ^{202}Hg=-1.34±0.34‰, Δ^{199}Hg=-0.02±0.06‰ and Δ^{200}Hg=-0.02±0.02‰ (n=7) in Chenqi catchment (Fig. 5b). The Hg isotope compositions of bedrock were δ^{202}Hg=-0.79±0.23‰, Δ^{199}Hg=0.05±0.05‰ and Δ^{200}Hg=0.01±0.03‰ (n=3) in Huilong catchment, and were δ^{202}Hg=-0.83±0.05‰, Δ^{199}Hg=0.17±0.07‰ and Δ^{200}Hg=0.04±0.01‰ (n=2) in Chenqi catchment. Compared with Hg isotope compositions of bedrocks in the other regions of the world, δ^{202}Hg was usually negative, and both Δ^{199}Hg and Δ^{200}Hg closd to 0 (Obrist et al. 2017). The slightly positive Δ^{199}Hg for carbonate rocks observed in the present study may be related to the material deposition-diagenesis process, but this need more evidence.

The Hg isotope composition of surface runoff in Huilong were δ^{202}Hg=-0.66 ± 0.27‰, Δ^{199}Hg=0.16 ± 0.13‰ and Δ^{200}Hg=0.03±0.04‰ (n=5), and those of groundwater were δ^{202}Hg=-0.42 ± 0.15‰, Δ^{199}Hg=0.05 ± 0.07‰ and Δ^{200}Hg=0.03±0.01‰ (n=4) (Fig. 5a). The Hg isotope compositions of surface runoff in Chenqi were δ^{202}Hg=-1.10 ± 0.23‰, Δ^{199}Hg=0.06 ± 0.15‰ and Δ^{200}Hg=0.02±0.08‰ (n=5), and those of groundwater were δ^{202}Hg=-1.38 ± 0.21‰, Δ^{199}Hg=-0.02 ± 0.10‰ and Δ^{200}Hg=0.00±0.02‰ (n=6) (Fig. 5b). The Hg isotopes of surface runoff retained the signatures of rainfall to a certain extent, especially

the positive Δ^{199}Hg, likely because the surface runoff in this area was formed within a short time after rainfall and then infiltrated rapidly. The Hg isotopes of groundwater were generally consistent with signatures of soil in the two catchments, suggesting sufficient exchange with soil Hg after precipitation entering the soil system.

Using the triple-mixing isotope model, it was estimated that soil Hg, rainfall Hg, and throughfall Hg contributed 84 ± 9%, 11 ± 9%, and 5 ± 12%, respectively, to groundwater Hg in Huilong, and 88 ± 12%, 5 ± 20%, and 7 ± 25%, respectively, in Chenqi. Thus, soil Hg was the main source for groundwater Hg. Surface fissures developed in karst areas and land use types may directly impact rainfall and throughfall Hg input to groundwater.

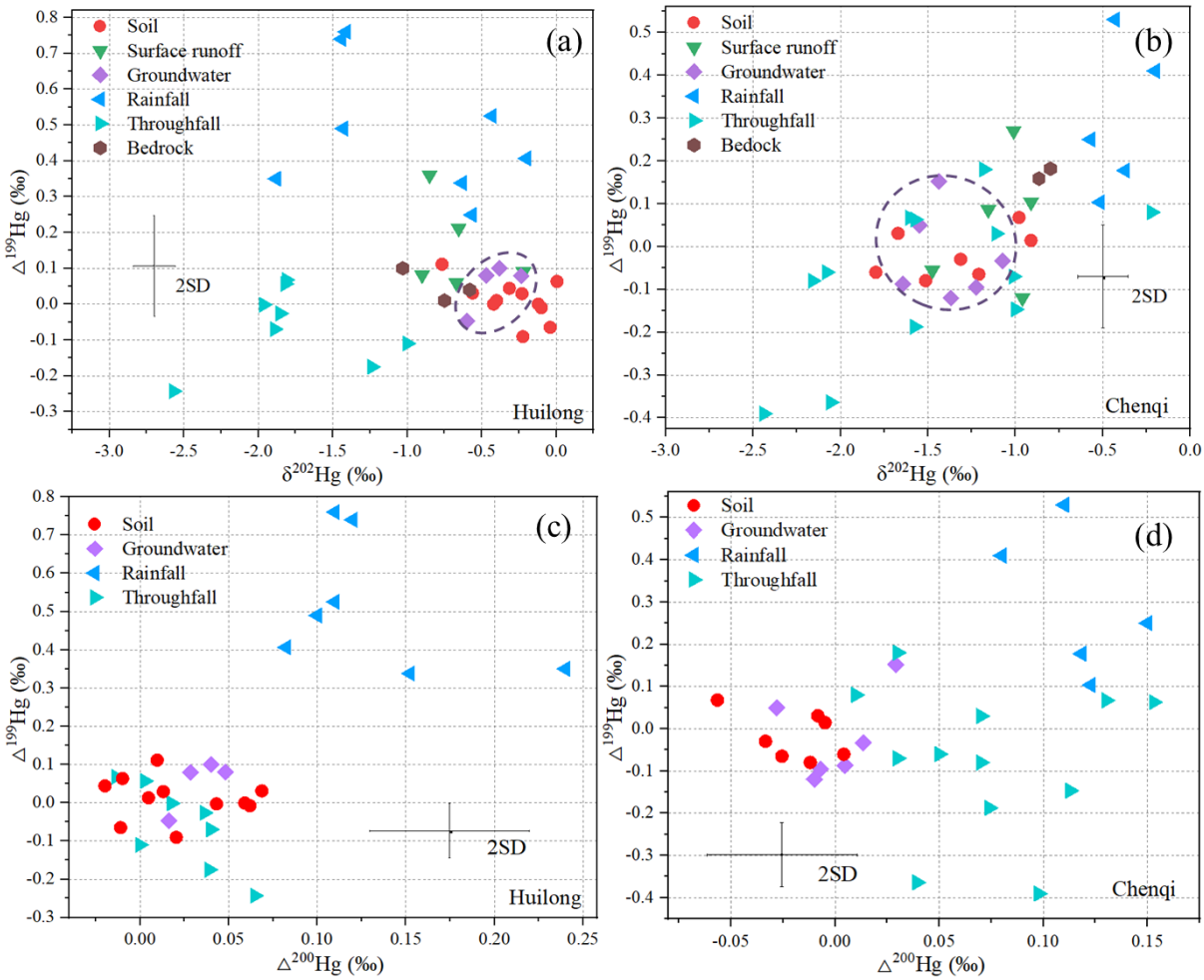

Fig. 5 The Hg isotope compositions of environmental media in Huilong and Chengqi catchments.

3.6 The implications of soil Hg transformation to karst groundwater safety

Due to the unique dual hydrologic structure of the area's karst system (characterized by both an above ground and underground flow field), the downward migration of soil Hg becomes a potential risk for regional groundwater security in karst areas with high Hg background concentrations, such as in Huilong catchment with a soil Hg pool as high as 44.4±4.2 g m^{-2}. Previous research documented that Hg-DOM and ionic Hg have relatively higher vertical mobility in soil (Gai et al. 2016). $Hg(SR)_2$ investigated in the present study has similar chemical properties to those of Hg-DOM reported in literature (Liu et al. 2019a). Fig. 6 shows an illustration of Hg migration and transformation in farmland and forest soil profiles in the Huilong catchment based on results from the present study and data reported in Xia et al. (2021a). The present study shows ionic Hg increases with increasing soil depth, and such an increase is stronger in forest soil (from 6.7% to 11.6%) than in farmland soil (from 4.2% to 10.7%), while $Hg(SR)_2$ decreases with soil depth, and the trend is stronger in farmlands (from 44.0% to 20.3%) than forests (from 39.3% to 34.5%). Soil moisture contents are likely higher in forest soils than farmland soils due to the higher canopy height of forests. The leaching effect of ionic Hg in forest soils is thus stronger, as seen in the stronger trend of its vertical migration. The input of forest litterfall provides continuous replenishment of organic matter in the understory soil, resulting in downward migration of $Hg(SR)_2$. At the catchment scale, Hg input flux from precipitation and output flux through runoff were 20.9±13.3 μg m^{-2} yr^{-1} and 21.6±0.93 μg m^{-2} yr^{-1}, respectively (Xia et al. 2021a). Soil Hg speciation and associated high levels of Hg fluxes in various hydrological processes suggest the potential risks of soil Hg migration to groundwater in this karst area. This was consistent with the results of Hg isotope source analysis for groundwater Hg.

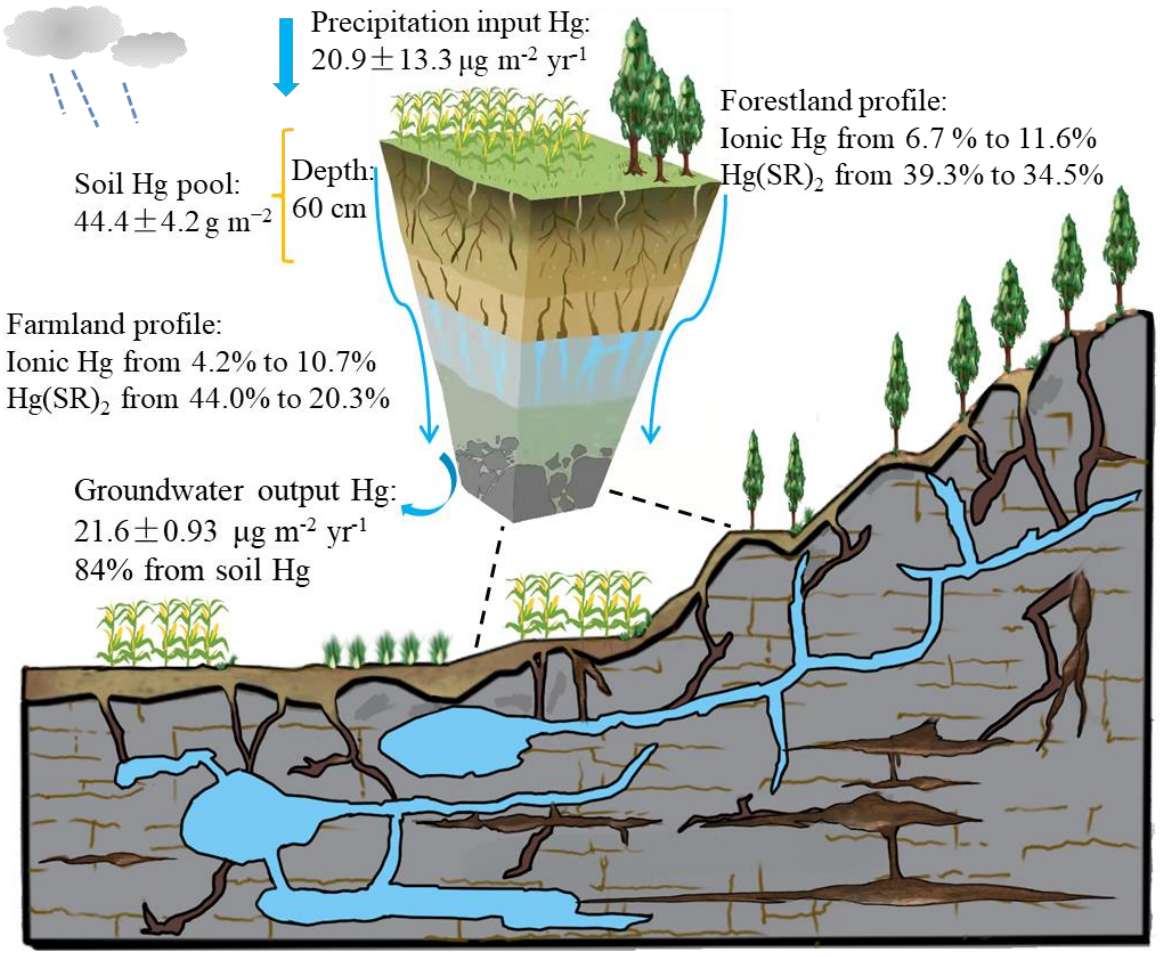

508

509 Fig. 6 Schematic illustration of Hg migration and transformation in farmland and forestland soil
510 profiles in Huilong catchment. The central soil column diagram was modified from Chorover et al.
511 (2007) and data of Hg input from precipitation and Hg output through runoff reported in Xia et al.
512 (2021a).

513

514 **4. Conclusions**

515 The extremely high soil Hg pool suggests a huge risk of Hg diffusion to the surrounding
516 environment in Huilong. From the perspective of the vertical migration of Hg in the soil
517 profile, compared with the farmland, the forest soil Hg realized a more obvious depletion.
518 SOM was closely related to the proportion of oxidizable Hg in the soil. During soil formation,
519 α-HgS, which is the primary Hg ore mineral, is gradually transformed into other mineral
520 types. The proportion of organic bound $Hg(SR)_2$ decreased while the proportion of ionic Hg
521 increased with increasing soil depth. It is particularly noteworthy that the tendency of ionic

Hg to increase with soil depth suggests an increased risk of soil Hg entering groundwater in karst areas with high Hg backgrounds. Soil Hg was the main Hg source for groundwater in this area. Therefore, the management and remediation of soil Hg pollution in such areas should not only focus on Hg at the soil surface, but also provide necessary monitoring and corresponding countermeasures for possible Hg migration to groundwater. Future research should take into account the migration and transformation of Hg in hydrological processes under different land use in karst areas.

Acknowledgement

This work was supported by the Program Foundation of the National Natural Science Foundation of China [41921004 and 42107497], the Strategic Priority Research Program of Chinese Academy of Sciences [XDB40000000], and the Guizhou Provincial Science and Technology Projects (QKHJC-ZK[2021]YB227).

References

Abu-Dieyeh MH, Alduroobi HM, Al-Ghouti MA. 2019. Potential of mercury-tolerant bacteria for bio-uptake of mercury leached from discarded fluorescent lamps. J Environ Manage 237:217-227.

Bavec Š, Gosar M. 2016. Speciation, mobility and bioaccessibility of hg in the polluted urban soil of idrija (slovenia). Geoderma 273:115-130.

Blum JD, Bergquist BA. 2007. Reporting of variations in the natural isotopic composition of mercury. Analytical and Bioanalytical Chemistry 388:353-359.

Blum JD, Sherman LS, Johnson MW. 2014. Mercury isotopes in earth and environmental sciences. In: Annual review of earth and planetary sciences, vol 42, Vol. 42, (Jeanloz R, ed), 249-269.

Bourdineaud JP, Durn G, Rezun B, Manceau A, Hrenovic J. 2020. The chemical species of mercury accumulated by pseudomonas idrijaensis, a bacterium from a rock of the idrija mercury mine, slovenia. Chemosphere 248:126002.

Chen J, Hintelmann H, Feng X, Dimock B. 2012. Unusual fractionation of both odd and even mercury isotopes in precipitation from peterborough, on, canada. Geochim Cosmochim Ac 90:33-46.

Chorover J, Kretzschmar R, Sparks LD. 2007. Soil biogeochemical processes within the critical zone. Elements 3:321-326.

Demers JD, Blum JD, Zak DR. 2013. Mercury isotopes in a forested ecosystem: Implications for air-surface exchange dynamics and the global mercury cycle. Global Biogeochem Cy 27:222-238.

Driscoll CT, Mason RP, Chan HM, Jacob DJ, Pirrone N. 2013. Mercury as a global pollutant: Sources, pathways, and effects. Environ Sci Technol 47:4967-4983.

Drott A, Bjorn E, Bouchet S, Skyllberg U. 2013. Refining thermodynamic constants for mercury(ii)-sulfides in equilibrium with metacinnabar at sub-micromolar aqueous sulfide concentrations. Environ Sci Technol 47:4197-4203.

Esbri JM, Bernaus A, Avila M, Kocman D, Garcia-Noguero EM, Guerrero B, et al. 2010. Xanes speciation of mercury in three mining districts - almaden, asturias (spain), idria (slovenia). J Synchrotron Radiat 17:179-186.

Fu., Feng X, Zhu W, Rothenberg S, Yao H, Zhang H. 2010. Elevated atmospheric deposition and dynamics of mercury in a remote upland forest of southwestern china. Environ Pollut 158:2324-2333.
Gai K, Hoelen TP, Hsu-Kim H, Lowry GV. 2016. Mobility of four common mercury species in model and natural unsaturated soils. Environ Sci Technol 50:3342-3351.
Gómez-Armesto A, Méndez-López M, Pontevedra-Pombal X, García-Rodeja E, Moretto A, Estévez-Arias M, et al. 2020. Mercury accumulation in soil fractions of podzols from two contrasted geographical temperate areas: Southwest europe and southernmost america. Geoderma 362:114120.
Gruba P, Socha J, Pietrzykowski M, Pasichnyk D. 2019. Tree species affects the concentration of total mercury (hg) in forest soils: Evidence from a forest soil inventory in poland. Sci Total Environ 647:141-148.
Gustin MS, Lindberg S, Marsik F, Casimir A, Ebinghaus R, Edwards G, et al. 1999. Nevada storms project: Measurement of mercury emissions from naturally enriched surfaces. Journal of Geophysical Research: Atmospheres 104:21831-21844.
Huang QH, Cai YL, Xing XS. 2008. Rocky desertification, antidesertification, and sustainable development in the karst mountain region of southwest china. Ambio 37:390-392.
Li K, Lin C-J, Yuan W, Sun G, Fu X, Feng X. 2019. An improved method for recovering and preconcentrating mercury in natural water samples for stable isotope analysis. Journal of Analytical Atomic Spectrometry 34:2303-2313.
Li X, Liang Z, Yang Z, Yang S, Wu L, Wang H, et al. 2021. Improvement and exploration of soil organic matter determination method. Modern agricultural science and technology 20:155-157 (In Chinese with English abstract).
Liu, Wang J, Feng X, Zhang H, Zhu Z, Cheng S. 2019a. Spectral insight into thiosulfate-induced mercury speciation transformation in a historically polluted soil. Science of The Total Environment 657:938-944.
Liu, Zhang Q, Ge S, Mason RP, Luo Y, He Y, et al. 2019b. Rapid increase in the lateral transport of trace elements induced by soil erosion in major karst regions in china. Environ Sci Technol 53:4206-4214.
Ma H, Cheng H, Guo F, Zhang L, Tang S, Yang Z, et al. 2022. Distribution of mercury in foliage, litter and soil profiles in forests of the qinling mountains, china. Environ Res 211:113017.
McLagan DS, Schwab L, Wiederhold JG, Chen L, Pietrucha J, Kraemer SM, et al. 2022. Demystifying mercury geochemistry in contaminated soil-groundwater systems with complementary mercury stable isotope, concentration, and speciation analyses. Environ Sci Process Impacts.
Monteiro Venturini A, Silvestre Dias NM, Gontijo JB, Yoshiura CA, da Silva Paula F, Meyer KM, et al. 2022. Increased soil moisture intensifies the impacts of forest-to-pasture conversion on methane emissions and methane-cycling communities in the eastern amazon. Environ Res:113139.
Nesbitt HW. 1979. Mobility and fractionation of rare earth elements during weathering of a granodiorite. Nature 279:206-210.
Nie LS, Liu XM, Wang XQ, Liu HL, Wang W. 2019. Interpretation of regional-scale distribution of high hg in soils of karst area in southwest china. Geochem-Explor Env A 19:289-298.
Obrist D, Agnan Y, Jiskra M, Olson CL, Colegrove DP, Hueber J, et al. 2017. Tundra uptake of atmospheric elemental mercury drives arctic mercury pollution. Nature 547:201-204.
Qiu G, Feng X, Wang S, Fu X, Shang L. 2009. Mercury distribution and speciation in water and fish from abandoned hg mines in wanshan, guizhou province, china. Sci Total Environ 407:5162-5168.
Qiu GL, Feng XB, Wang SF, Mao TF. 2006. Mercury contaminations from historic mining to water, soil and vegetation in lanmuchang, guizhou, southwestern china. Sci Total Environ 368:56-68.
Quintanilla-Villanueva GE, Villanueva-Rodríguez M, Guzmán-Mar JL, Torres-Gaytan DE, Hernández-Ramírez A, Orozco-Rivera G, et al. 2020. Mobility and speciation of mercury in soils from a mining zone in villa hidalgo, slp, mexico: A preliminary risk assessment. Appl Geochem 122:104746.
Ravel B, Newville M. 2005. Athena, artemis, hephaestus: Data analysis for x-ray absorption spectroscopy using ifeffit. J Synchrotron Radiat 12:537-541.

611 Santos JCBd, Le Pera E, Oliveira CSd, Souza Júnior VSd, Pedron FdA, Corrêa MM, et al. 2019. Impact of
612 weathering on ree distribution in soil-saprolite profiles developed on orthogneisses in borborema
613 province, ne brazil. Geoderma 347:103-117.
614 Silva-Filho EV, Machado W, Oliveira RR, Sella SM, Lacerda LD. 2006. Mercury deposition through
615 litterfall in an atlantic forest at ilha grande, southeast brazil. Chemosphere 65:2477-2484.
616 Soleh Setiyawan A, Effendi AJ, Lestari V, Irsyad M, Dwi Ariesyady H, Nastiti A, et al. 2020. Optimizing
617 soil washing remediation of mercury contaminated soil using various washing solutions and
618 solid/liquid ratios. E3S Web of Conferences 148:05004.
619 Sun JL, Zou X, Ning ZP, Sun M, Peng JQ, Xiao TF. 2012. Culturable microbial groups and thallium-
620 tolerant fungi in soils with high thallium contamination. Sci Total Environ 441:258-264.
621 Sun ZY, Wen XF, Wu P, Liu Y, Pan QZ. 2019. Excessive degrees and migration characteristics of heavy
622 metals in typical weathering profiles in karst areas. Earth and Environment 47:50-56(In Chinese with
623 English abstract).
624 Teršič T, Biester H, Gosar M. 2014. Leaching of mercury from soils at extremely contaminated
625 historical roasting sites (idrija area, slovenia). Geoderma 226-227:213-222.
626 Wang J, Shaheen SM, Anderson CWN, Xing Y, Liu S, Xia J, et al. 2020. Nanoactivated carbon reduces
627 mercury mobility and uptake by oryza sativa l: Mechanistic investigation using spectroscopic and
628 microscopic techniques. Environ Sci Technol 54:2698-2706.
629 Wang SF, Feng XB, Qiu GL, Wei ZQ, Xiao TF. 2005. Mercury emission to atmosphere from lanmuchang
630 hg-tl mining area, southwestern guizhou, china. Atmos Environ 39:7459-7473.
631 Wang X, Bao Z, Lin C-J, Yuan W, Feng X. 2016. Assessment of global mercury deposition through
632 litterfall. Environ Sci Technol 50:8548-8557.
633 Wang X, Yuan W, Feng X, Wang D, Luo J. 2019. Moss facilitating mercury, lead and cadmium
634 enhanced accumulation in organic soils over glacial erratic at mt. Gongga, china. Environ Pollut
635 254:112974.
636 Wiederhold JG, Skyllberg U, Drott A, Jiskra M, Jonsson S, Bjorn E, et al. 2015. Mercury isotope
637 signatures in contaminated sediments as a tracer for local industrial pollution sources. Environ Sci
638 Technol 49:177-185.
639 Xia J, Wang J, Zhang L, Wang X, Yuan W, Anderson CWN, et al. 2021a. Significant mercury efflux from
640 a karst region in southwest china - results from mass balance studies in two catchments. Sci Total
641 Environ 769:144892.
642 Xia J, Wang J, Zhang L, Wang X, Yuan W, Zhang H, et al. 2021b. Mass balance of nine trace elements
643 in two karst catchments in southwest china. Sci Total Environ 786:147504.
644 Xiao Q, Dong Z, Han Y, Hu L, Hu D, Zhu B. 2021. Impact of soil thickness on productivity and nitrate
645 leaching from sloping cropland in the upper yangtze river basin. Agriculture, Ecosystems &
646 Environment 311:107266.
647 Xie S, Yuan S, Liao P, Tong M, Gan Y, Wang Y. 2017. Iron-anode enhanced sand filter for arsenic
648 removal from tube well water. Environ Sci Technol 51:889-896.
649 Yin R, Gu C, Feng X, Hurley JP, Krabbenhoft DP, Lepak RF, et al. 2016. Distribution and geochemical
650 speciation of soil mercury in wanshan hg mine: Effects of cultivation. Geoderma 272:32-38.
651 Yin., Feng X, Shi W. 2010. Application of the stable-isotope system to the study of sources and fate of
652 hg in the environment: A review. Appl Geochem 25:1467-1477.
653 Zhao M, Zeng C, Liu Z, Wang S. 2010. Effect of different land use/land cover on karst
654 hydrogeochemistry: A paired catchment study of chenqi and dengzhanhe, puding, guizhou, sw china.
655 J Hydrol 388:121-130.

656

657